Journal of Applied Fluid Mechanics, Vol. 17, No. 5, pp. 1112-1128, 2024.
Available online at www.jafmonline.net, ISSN 1735-3572, EISSN 1735-3645.
https://doi.org/10.47176/jafm.17.05.2169

Integral Airfoil Generation of Multi-rotor Aircraft Based on Optimization of Upper Wing Contour and CFD Simulation

Z. Wang[1], Y Zhu[2], Q. Yuan[3†], W. B. Gu[2] and X. B. Xie[2]

[1] *Army Command Academy of PLA, Jiangsu Nanjing 210045, China*
[2] *Army Engineering University of PLA, Nanjing, Jiangsu, 210007, China*
[3] *Southwest University of Science and Technology, Mianyang, Sichuan, 621010, China*

†Corresponding Author Email: yuanqi@swust.edu.cn

ABSTRACT

Regarding the airfoil optimization design of multi-rotor unmanned aerial vehicles, this paper proposes an integral airfoil design method based on upper airfoil contour optimization. Firstly, by designing concave descent input curves with 0-1 distribution, the upper arc of different optimized airfoils is obtained using the Tangent circles method. Secondly, an integral airfoil generation method is developed after establishing the middle arc. As the upper and lower arcs of different shapes are randomly combined, various airfoil profiles are obtained by random assortment. Finally, the effectiveness and accuracy of the designed airfoil are validated through Python programming. The airfoil is generated by the *XFOIL* program, and the optimal airfoil is output with a lift-to-drag ratio as the target. Meanwhile, an accurate Fluent analysis model is established, and a comparison verification is conducted on the data with the attack angle falling within [-8.02, 12.04] and lift-to-drag ratio falling within [-50, 100]. After Fluent modeling of the designed airfoil, the Euclidean distance between the calculated angle-lift-drag ratio data curve and the data curve tested by the wind tunnel is 0.0331, while the Euclidean distance between the simulated data in the literature and the wind tunnel data is 0.0408. It indicates that our precise model achieves 18.9% higher accuracy than the literature model. Testing and verification results indicate that our designed airfoil based on upper arc optimization and its corresponding airfoil library can meet the design requirements for the aerodynamic performance of airfoils in practical applications. It provides a valuable reference for the development of airfoil design, optimization, and generation methods.

Article History

Received July 17, 2023
Revised November 13, 2023
Accepted December 11, 2023
Available online February 24, 2024

Keywords:

Airfoil design
Parameterization method
Upper airfoil contour optimization
Computational fluid dynamics
Aerodynamic performance

1. INTRODUCTION

Wing profile optimization plays a crucial role in enhancing the transportation efficiency, flight quality, and aerodynamic performance of unmanned aerial vehicles, and it is an essential element for generating the required lift for aircraft navigation and various flight maneuvers while ensuring stability and maneuverability. Despite the presence of various wing profile series and the construction of wing profile databases by many countries, there does not exist nor is it possible to have a single super wing profile that is universally applicable to all airflow conditions and flight states, while meeting all desired expectations. The geometric description of the wing profile significantly affects the efficiency of wing profile optimization, so it is crucial and necessary to investigate the aerodynamic shape of wing profiles, explore optimization design methods, and develop high-performance wing profiles.

In recent years, for the development of wing design and optimization methods, the main themes and key technologies of related research mainly focus on the following three aspects:

(1) Airfoil design method based on sparse weighted parameters

The current research hotspot is the adoption of wing profiles or the development based on existing wing profiles. The design method for the wing profile of the current rotorcraft mainly reduces the dimension of the design space by using parameterization methods. Early parametric design methods for wing profile optimization usually employed the convex function (Bump) method

(Lepine et al., 2001; Bharadwaj et al., 2016). The basic function is weighted and superimposed on the basic airfoil, and the shape of the airfoil is changed by the control factor.

This type of method requires only a few control parameters to optimize the upper and lower surfaces of the airfoil, and any airfoil can be utilized as the initial airfoil for optimization. However, this method also has obvious defects: it cannot guarantee the smoothness of the airfoil and has a significant impact on the aerodynamic characteristics. Thus, it is necessary to make a balance and compromise between computational simplicity and aerodynamic performance.

(2) More complicated parameterized airfoil design method

The wing profile optimization design method that utilizes fewer weighting parameters in its early stages is the opposite. In recent years, the advancement of high-performance computing hardware and computer-aided design (CAD) has prompted the use of parameterized curves for wing profile design, which can automatically maintain the smoothness of the wing profile. Currently, there are three main categories of parameterization methods for wing profiles. The first category of method is based on basis functions, which are combined linearly to form smooth geometric perturbations and superimposed to obtain new wing profile curves. Representatives of such methods are the Hicks-Henne-type function method (Hicks & Henne, 1978; Zhou et al., 2021), Wagner-type function method (Ramamoorthy & Padmavathi, 1977), polynomial-type function method (Lee & Eyi, 1992), and class function/shape function transformation (CST) parametrization method (Kulfan, 2008; Akram & Kim, 2021; Kou et al., 2023). The second category of method uses spline curves, such as B-spline (Wang et al., 2004; Nemec et al., 2004; Leung & Zingg, 2009; Fujii & Dulikravich, 2013; Zakaria et al., 2021), non-uniform rational B-spline (NURBS) (Lepine et al., 2001; Guibault et al., 2002; Painchaud-Ouellet et al., 2006; Sevilla et al., 2011; Li et al., 2015; Aghabeigi et al., 2022), Bezier curves (Mengistu & Ghaly, 2002; Prautzsch et al., 2002), etc. To approximate the wing profile curve. The third category of method is based on wing profile characteristic parameters (e.g., maximum camber position) (Zhang et al., 2018), and the wing profile curve is usually represented with edge radius, maximum thickness position, and trailing edge angle. Different parameterized geometric models have different abilities in describing the optimization search space, and a good parametrization method not only fully captures the small changes in the airfoil surface but also enhances the optimization efficiency.

Therefore, the main issue restricting the flexibility of the airfoil design is that more control parameters are required to achieve higher efficiency. However, an excess of parameters can lead to redundancy, which does not always guarantee a smoother generation of airfoils.

(3) Airfoil optimization design method combined with intelligent algorithms

With the improvement of computer performance and the development of numerical methods, research on wing optimization design tends to combine wing parameterization with optimization algorithm simulation to obtain the optimal wing shape. Emerging intelligent algorithms, such as deep learning (Li et al., 2022), neural networks (Khurana et al., 2008; Sun et al., 2015; Sekar et al., 2019), genetic algorithms (Vicini & Quagliarella, 1997; Gardner & Selig, 2003; Huang et al., 2006), and multi-objective networks, are favored by researchers and have been applied in wing generation studies. For instance, Buckley and Zingg (Buckley & Zingg, 2013) developed a multi-point optimization design method based on Pareto fronts by calculating the weighted objective function, which can not only optimize the aerodynamic shape of supersonic civil aircraft but also optimize the long-distance and long-endurance flight performance of unmanned aerial vehicles (UAV). Based on CFD technology, Chen and Agarwal (Chen & Agarwal 2014) used multi-objective genetic algorithms in the optimization process to eliminate shock waves and improve lift coefficients for supersonic wing shape optimization.

Though this approach of using intelligent algorithms for wing optimization is feasible and effective, it needs a large dataset of wing shapes in the wing library to train the intelligent algorithms, and the quality of the wing shapes in the library directly affects the quality of the wing shapes designed by the intelligent algorithms.

Therefore, considering the aforementioned issues and the defects of existing research, this paper proposes a computationally efficient and high-performance method for rapid airfoil generation and optimization. In the design process, a unique design approach is adopted, which consists of the following three aspects:

(1) Starting from the input curve, the upper arc generation process for the airfoil is optimized to address the optimization issue of specific airfoils from the source (corresponding to Section 3 of the article).

(2) Based on the designed upper arc, numerous specific samples are generated rapidly by combining programming languages with airfoil library generation, thus solving the problem of generating massive airfoil library data from a methodological perspective (corresponding to Section 4 of the article).

(3) By taking aerodynamic parameters as optimization constraints, specific airfoils are selected rapidly using Xfoil software and precise airfoil models, are then they are generated using Fluent. These models are compared and validated with wind tunnel test data to verify the practicality and effectiveness of the designed airfoil (corresponding to Section 5 of the article).

2. OVERVIEW OF THE AIRFOIL DESIGN PROCESS

A typical mainly consists of four parts: leading edge, trailing edge, upper surface or suction side, and lower surface or pressure side. The airfoil is determined by several key features, including camber, thickness, leading edge radius, and trailing edge angle. Nevertheless, these are all traditional airfoil characteristics, and many other specific parameters exist, such as the position of the center of the incircle of the leading edge radius, the angle

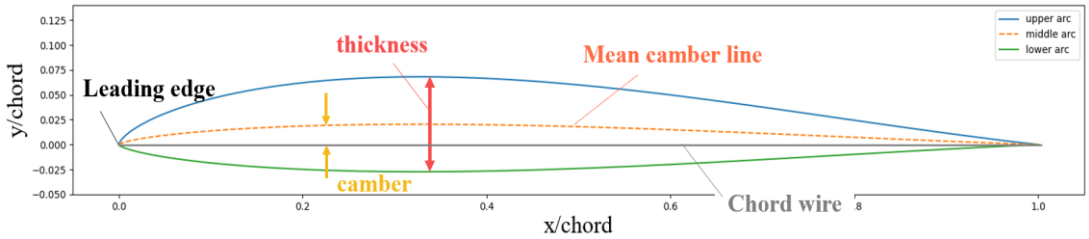

Fig. 1 Typical airfoil structure

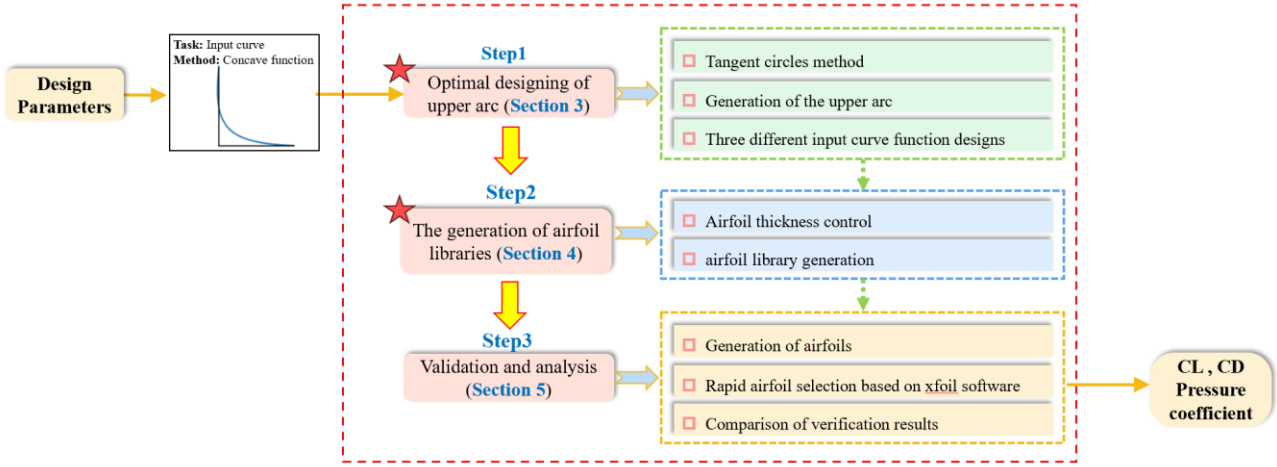

Fig. 2 Airfoil design framework

between the chord line and the line connecting the center of the incircle and the leading edge point, the ratio of the transverse coordinate of the maximum thickness point to the chord length, as well as the angle between the airfoil shape and the chord line of the upper and lower surfaces. All these factors affect the overall shape of the airfoil and thus its aerodynamic characteristics. The typical airfoil structure is illustrated in Fig. 1, with its overall shape composed of upper and lower arc lines, and some detailed features such as thickness are presented in the figure. In this section, a new airfoil generation algorithm is proposed based on mathematical methods and geometric thinking, combined with Python programming software. This algorithm considers the main factors that affect the aerodynamic characteristics of the airfoil.

In this section, the process of developing a multidisciplinary design framework for modeling and analysis of different airfoil shapes is introduced. Given the description of each step in the airfoil design process, this framework performs an automated evaluation of the airfoil based on optimized aerodynamic performance metrics. The term "automated evaluation" refers to the use of programming languages to jointly utilize the software and execute it in batch mode. The developed design framework is shown in Fig. 2.

Step 1: The optimal design of the upper arc, which will be described in Section 3. The upper arc of the airfoil is generated by utilizing the Tangent circles method and exploiting the distribution characteristics of concave functions and binary distribution input curves, such as power functions and polynomials.

Step 2: The generation of airfoil libraries, which will be described in Section 4. Firstly, the arc in the airfoil is designed. Since the mid arc is located between the upper and lower arcs, the coordinates of the lower arc can be obtained by interpolating the coordinates of the upper and mid arcs, thereby ensuring the smoothness of the lower arc. Then, the overall airfoil and airfoil library are generated, and the complete airfoil curve is obtained by combining the upper and lower arcs. Subsequently, the airfoil library is formed through the random configuration of different upper and lower arcs.

Step 3: Validation and analysis, which will be described in Section 5. Firstly, the wind tunnel data of reference literature on airfoils is taken for comparison and validation. Using Python language, numerous feature airfoils with different thickness characteristics are generated. Then, the XFOIL program is invoked using Python for rapid selection, whereby non-converging airfoil calculation samples are removed. Next, the lift-to-drag ratio characteristics of airfoils with different thicknesses are compared and analyzed to determine the optimal airfoil that exhibits the highest consistency with the aerodynamic characteristics of the target airfoil in the wind tunnel data. Finally, the selected airfoil is validated using Fluent software to evaluate its consistency with the GAW-1 airfoil curve in the reference literature, and the curve-fitting error is calculated. In this process, XFOIL can be also used for calculations, but singular points may appear, whereas this issue can be addressed by using Fluent. A comparison of the results from the two software programs is provided.

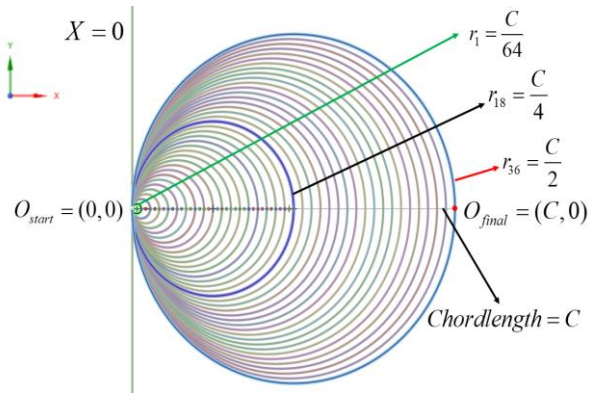

Fig. 3 Tangent circles with different leading-edge radii

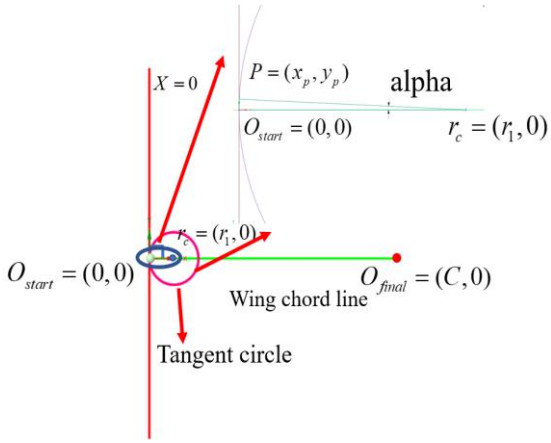

Fig. 4 Determination of arc Angle

3. OPTIMAL DESIGNING OF UPPER ARC

In this section, a new algorithm is proposed for generating the contour line of the upper airfoil, according to the main factors that affect the aerodynamic characteristics of the airfoil (the method of arc angle intersection of the circle inner tangent radius).

3.1 Upper arc Design Idea

As mentioned above, many feature factors need to be considered in the design of airfoil parameters. Research on airfoil parameter design has indicated that the position of the inflection point on the upper arc and the thickness of the airfoil have a significant impact on the smoothness and aerodynamic performance of the airfoil. In this section, by using the method of "intersection of radius and arc angle of an inscribed circle", the upper arc of the airfoil, which meets the design requirements, is constructed by changing the radius and arc angle of the inscribed circle. The construction process involves the following three steps.

3.1.1 Tangent Circles Method

The outer contour of the upper arc is generated using the method of "intersection of radius and arc angle of an inscribed circle". By changing the radius and angle of the tangential circle, the corresponding coordinate values of the front edge radius and angle in a two-dimensional Cartesian coordinate system are obtained, where the initial outer contour of the upper arc is constructed using a parameter equation.

A two-dimensional Cartesian coordinate system is established, with the origin $O_{start}=(0,0)$ at the leading edge and the chord as the *X*-axis of the wing. The origin is the starting point of the upper arc contour, and the chord length of the airfoil is set to *C*. The coordinate of the endpoint O_{final} of the upper arc contour is (*C*,0). The center of the tangent circle is placed within the space of the *X*-axis airfoil string, and the line $x = 0$ is externally tangent to all tangent circles, as illustrated in Fig. 3. The range of the tangent circle's radius R_x is $[0,\frac{C}{2}]$, where $R_x=0$ corresponds to a point at the center (0,0). When $R_x=\frac{C}{2}$, it corresponds to the circle with $r_{36}=\frac{C}{2}$ in the diagram, with the center at $[\frac{C}{2},0]$, and this circle also passes through points (0,0) and (C,0). Additionally, $r_1=\frac{C}{64}$ and $r_{18}=\frac{C}{4}$ represent tangent circles with different radii in the diagram.

3.1.2 The Generation of Upper Arc

The determination of the angular arc is shown in Fig. 4. A tangent circle with an arbitrary center $r_c=(r_1,0)$ is selected, and an arbitrary reference angle *alpha* is selected within the tangent circle, where *alpha* is given as $\angle \mathrm{Pr}_c O_{start}$. Given a known radius of the tangent circle, the coordinate values of point *P* corresponding to the circle can be obtained using the parametric coordinate equation of the circle.

The cartesian coordinates of point *P* are solved as follows,

$$\begin{cases} x_p = r_1 + r_1\cos(\pi - alpha) \\ y_p = r_1\cos(\pi - alpha) \end{cases} \tag{1}$$

where, x_p represents the abscissa of point *P*, y_p represents the ordinate of point *P*, and r_1 denotes the abscissa value of the center of the circle. According to the geometric properties, it can be determined that $alpha \in [0,\pi]$. When determining the values of R_x and *alpha*, there must exist one and only one radius and one angle for which the tangent of the arc on the airfoil is parallel to the *x*-axis, i.e., the derivative is zero, and the position of this point is closely related to the curvature of the arc. Then, within their respective ranges, R_x and *alpha* are divided into 36 equal parts in ascending order, and one-to-one correspondences are established to form a new set *RA*=(R_x, *alpha*). By using the parametric equations of the circle, the coordinates (x_i, y_i) of the points on the arc of the airfoil in the Cartesian coordinate system corresponding to each pair (R_x, *alpha*) in *RA* are calculated, as demonstrated in Fig. 5. It can be seen that the upper arc has good smooth transition characteristics. However, the abscissa of the point with the maximum curvature of this curve is located

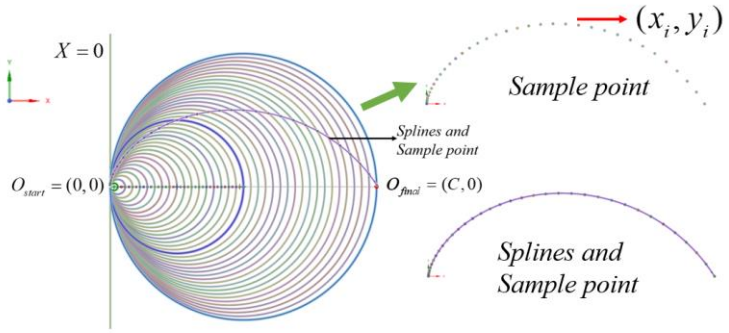

Fig. 5 Spline curve

at $\frac{C}{2}$, which does not meet the design requirements of the airfoil curvature (Zhang et al., 2018). Therefore, it is necessary to further optimize the distribution of sample points on this curve.

The generated *P* points are connected, and the *P* points and spline curves are illustrated in Fig. 5. It can be found that the curve possesses very good smooth transition characteristics, but the horizontal coordinate of the maximum curvature point of the curve is at the position of $\frac{C}{2}$, which has a curvature that does not meet the airfoil design conditions (Zhang et al., 2018), so the distribution of sample points of the curve should be further optimized.

3.2 Comparison of Optimization Results of Three Different Input Curves

For wing design, it is more reasonable to make the horizontal coordinate of the maximum point of the upper arc curvature range between $(0,\frac{C}{2})$, as it can improve the aerodynamic and structural characteristics of the wing. To optimize the distribution of sample points that make up the upper arc of the wing, it is necessary to investigate the relationship between the distribution characteristics of the sample points and R_x, *alpha*. To obtain the sample point data under different distributions of the upper arc of the wing, the wing coordinates are standardized, with the maximum and minimum values of the horizontal coordinate being 1 and 0, respectively. Therefore, a concave function input curve with a distribution range between (0, 1) can be adopted to design the sample points on the upper arc of the wing. The concave function input curve with a distribution range between 0 and 1 is taken as a distribution control coefficient. Therefore, to generate concave function curves and explore their influence on the characteristics of the upper arc, this paper analyzes the power function, three-point polynomial fitting function, and user-defined function curves to select the most suitable concave function input curve for the 0-1 distribution.

3.2.1 The Power Function Optimizes the Distribution of Arc Points on the Airfoil

To obtain the sample point data under different distributions of the upper airfoil contour lines, functions between (0,1) are employed to optimize the sample point distribution of the spline curve.

The expression of the power function is shown in formula (2),

$$y = x^a \tag{2}$$

If $y \in [0,1]$, where the range of x is $x \in [0,1]$, and C=100, then the function is monotonically increasing when $a > 0$. Thus, the value of 'a' determines the variation trend of the power function curve, and in this case, the data transformation for R_x and *alpha* can be represented by formula (3):

$$\begin{cases} R_x = y*C \\ alpha = y*\pi \end{cases} \tag{3}$$

In the following, the progress of choosing the value of a is discussed:

(1) Calculation interval of 'a'

Firstly, the interval $[0.1,3]$ is taken as an initial range for the calculation to find out how the value of 'a' affects the distribution of sample points on the contour line of the upper arc. Given a step size of 0.1, the power function curve is shown in Fig. 6, where the position of the triangle point corresponds to the maximum curvature point of the curve.

Dividing the power function curve into 200 equal parts leads to 200 control points on the upper arc line. Reversing the order of these points yields a monotonically decreasing function. By using the aforementioned geometric and parametric equations, the coordinates of each point on the upper arc line and the outline of the upper wing surface are comprehensively derived, as illustrated in Fig. 7.

(2) Influence on upper airfoil under different values of 'a'

By taking all the points on the upper arc in Fig. 7 where the derivative is equal to zero, Fig. 8 is plotted. From the upper arc in the figure, it can be seen that when $a < 0.5$, the wing profile curve exhibits poor continuity, mainly characterized by a significant lack of continuity in the trailing edge. For $0.4 < a \leq 3$, the abscissa of the points, where the change rate of the upper arc is zero, shows a decreasing trend as a increases. When $a \leq 1$, the points

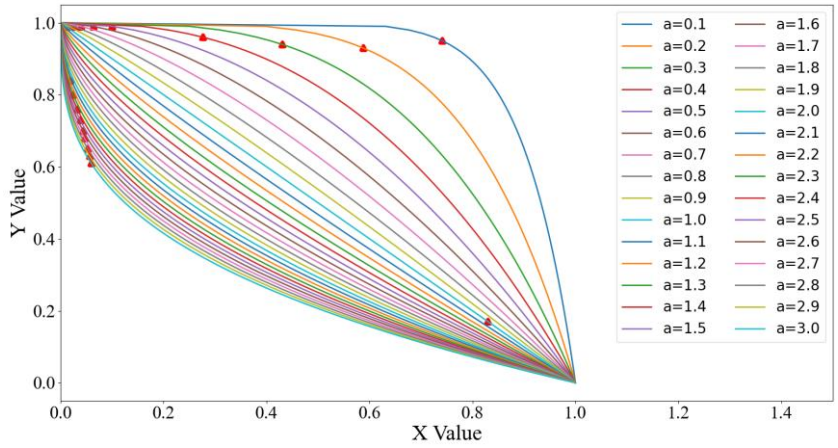

Fig. 6 Power function curves of different *a* values

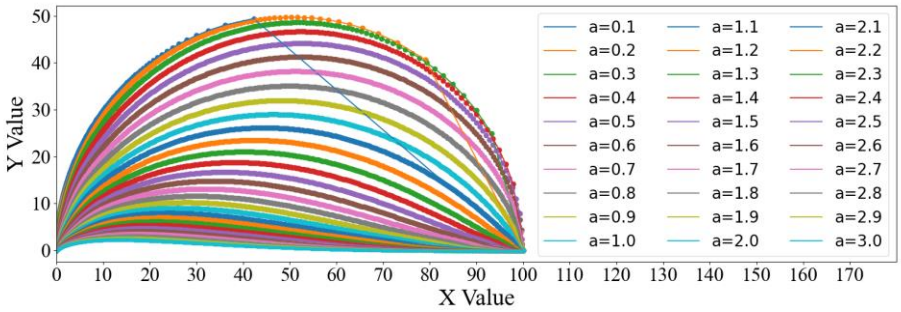

Fig. 7 Contour line of the upper airfoil

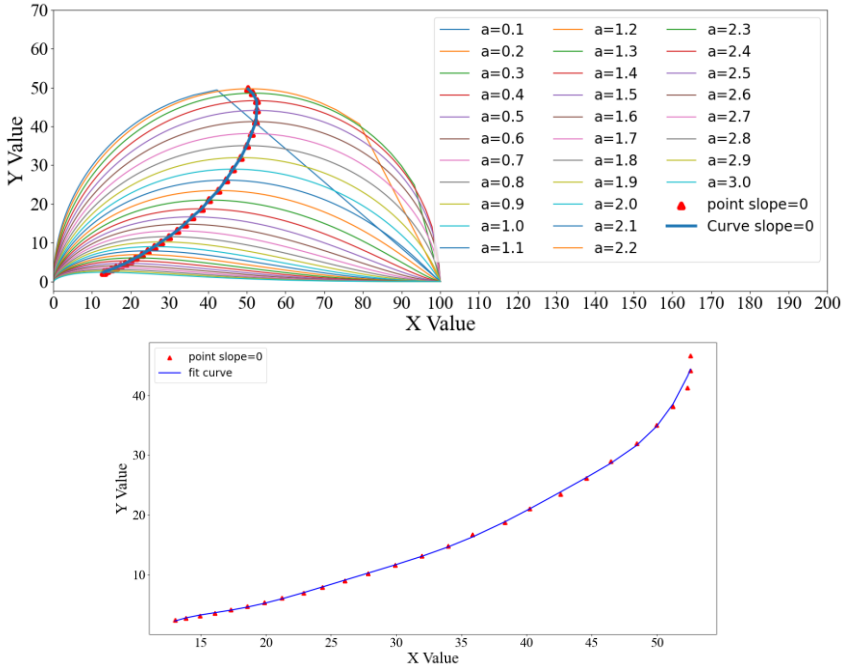

Fig. 8 Points for which the derivative of the contour line of the upper airfoil is 0

where the derivative of the upper arc is zero approach the trailing edge of the upper arc, and this contradicts the distribution pattern of aerodynamic characteristics. Therefore, curves within this range are discarded. Only when $a > 1$, i.e., when the input function curve is located below the line $y = x$, the abscissa of the points for which the change rate of the curve is zero approaches the range $(0, \frac{C}{2})$, providing a constraint for subsequent optimization of the upper arc of the wing profile.

In particular, when a=3.5, the spline curve shown in Fig. 9 can be obtained. The curve in this case is extremely unreasonable, and the ordinate values of sample points at the rear edge of the upper airfoil contour line are almost equal, which does not meet the airfoil selection criteria.

The function corresponding to the fitting curve is expressed below,

$$y = A \times B \tag{4}$$

$$A = \begin{pmatrix} 1.660\text{e-}08 \\ -3.603\text{e-}06 \\ 3.250\text{e-}04 \\ -1.578\text{e-}02 \\ 4.440\text{e-}01 \\ -7.203\text{e+}00 \\ 6.277\text{e+}01 \\ -2.25\text{e+}02 \end{pmatrix}, B = \left(x^7, x^6, x^5, x^4, x^3, x^2, x, 1\right) \tag{5}$$

where A is an 8×1 matrix containing the coefficients of independent variables of the polynomials, and B is a 1×8 matrix containing the independent variable of the polynomials.

In particular, when a=3.5, the spline curve as shown in Fig. 9 can be obtained. It can be seen that the upper arc generated in this case is extremely unreasonable, and the ordinate values of the sample points at the back edge of the upper arc are almost equal, which does not meet the airfoil selection criteria.

(3) The more focused interval of 'a'

To ensure the smoothness of the upper airfoil contour and the rationality of the data, a comprehensive consideration is made, and a value of $a \in [1.5, 2.54]$ is chosen, with the interval determined according to specific requirements. Assuming a step size of 0.08, the generated upper arc spline curve is shown in Fig. 10. It can be observed that the generated upper arc is relatively reasonable, but it exhibits a relatively singular upper arc feature.

3.2.2 Function Curve Features Are Fitted with Given Control Points

Due to the great functional limitations of power functions, a reverse control method using given control points can be utilized to fit a polynomial curve function with multiple points. The desired functional shape of the curve on the airfoil can be selected by choosing appropriate points, enabling control over the curve of the arc. In this section, polynomial functions are used to obtain the solution, and three polynomial control points are used to describe the fitting function curve, thereby ensuring a gradual decay in the coordinates of the control points and that the control points are below the line $y = x$. The expression for the control points is given in equation (6).

$$\begin{aligned} P_1 &= (0,1) \\ P_2 &= (P_{2x}, P_{2y}) \\ P_3 &= (1,0) \end{aligned} \tag{6}$$

where P_2 is a randomly generated point in (0,1), and it is located under the line $y = x$. The horizontal and vertical coordinates P_{2x} and P_{2y} of point P_2 satisfy:

$$P_{2y} = random(0,1) \tag{7}$$

$$P_{2x} = (1 - P_{2y}) * \tan(\alpha) \tag{8}$$

$$\alpha = random(0, \frac{\pi}{4}) \tag{9}$$

Using Python programming, a quadratic polynomial fitting is performed on three control points to obtain the function equation, as shown in Fig. 11. In the figure, $P_i = (x_i, y_i)$ is the intersection point of the curve and the line y=0, and the other parameter definitions have been described previously.

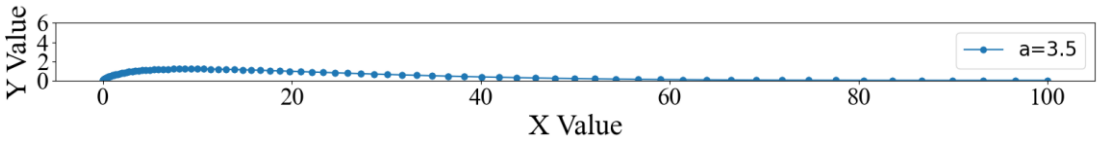

Fig. 9 Spline curve of upper airfoil contour when a=3.5

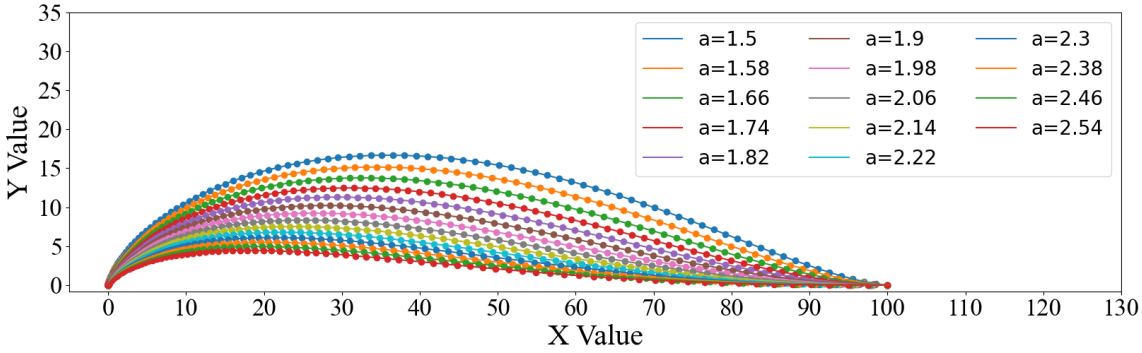

Fig. 10 Spline curve of the upper wing surface when $a \in [1.5, 2.54]$

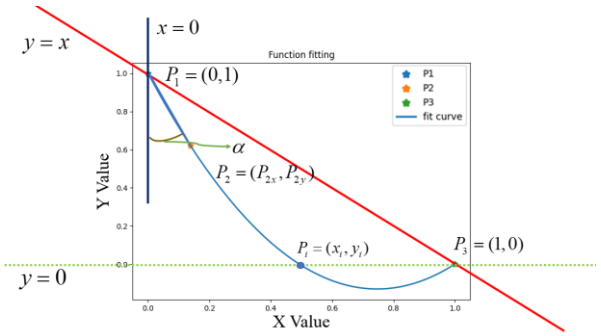

Fig. 11 Quadratic polynomial fitting control points

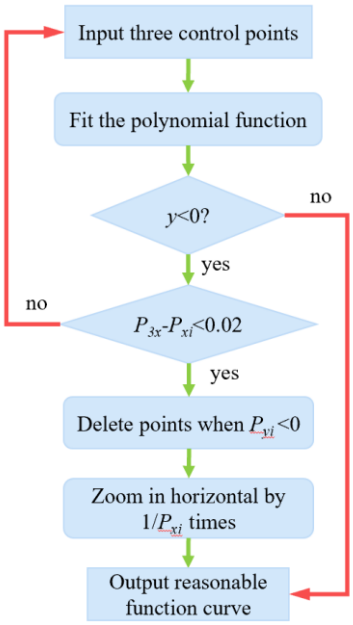

Fig. 12 Optimization of the control point function

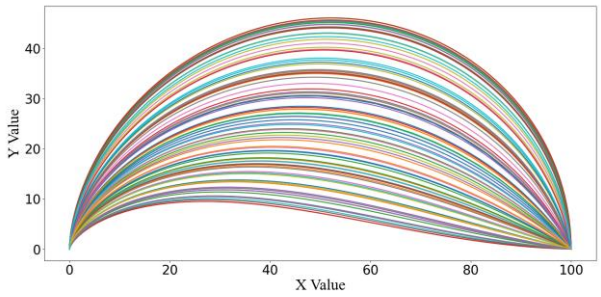

Fig. 13 Upper arc (uncontrolled random points)

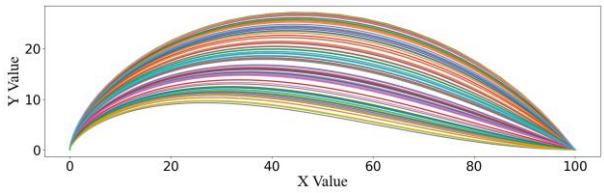

Fig. 14 Upper arc (control random points)

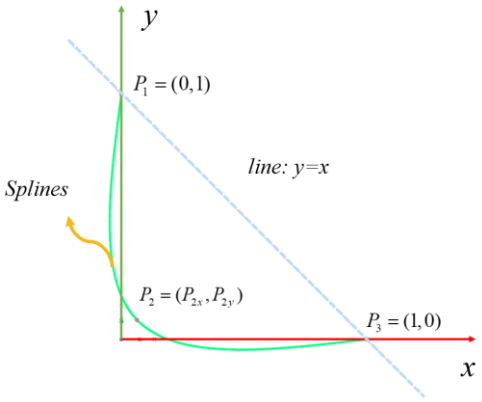

Fig. 15 Three-point control spline curve

It is obvious that point P_2 is located below the line $y = x$. However, there is an issue with the fitting curve. As indicated by the curve below the line $y = 0$ in Fig. 11, the region where P_iP_3 is negative is unreasonable in terms of upper arc design. According to computational theory, this directly leads to negative bending in the upper arc. Therefore, an optimization algorithm needs to be used here, and its basic idea is to iteratively evaluate and remove the negative region within the curve and then perform a scaling transformation on the remaining curve. The scaling ratio is defined as the ratio between the abscissa of P_3 (P_{x3}=1) and the abscissa of P_i (P_{xi}) in the flowchart. This ensures that both the x and y values fall within the correct and reasonable range. The basic flowchart is demonstrated in Fig. 12.

The calculated values (y) obtained by fitting a quadratic polynomial are used for the theoretical calculation to generate 100 upper arc lines, as shown in Fig. 13. The randomness of the data points is controlled to make them fall below the line $y = x$, resulting in the upper arc lines, as shown in Fig. 14. The optimized upper arc lines demonstrate better control effectiveness compared to the power function.

3.2.3 Three Points Control Spline Curve

According to the method for generating the upper arc curve of the airfoil in this paper, the three-point control spline curve generation method is employed to optimize the input function. The algorithm for generating the three control points is consistent with that introduced in Section 3.1.2. The following curve is an exception input distribution spline curve, so the following mainly discusses the case where the input spline curve has a negative region, as shown in Fig. 15.

If the interval points of the input spline curve are not processed, the upper arc is directly generated, as shown in Fig. 16.

When y is less than zero, the corresponding upper curve first moves downward and then upward, and it may intersect with the chord line at both ends of the airfoil, making the shape of the leading edge highly unreasonable. Therefore, the distribution of input spline curves has a significant impact on the upper curve. Consequently, it is necessary to optimize and reconstruct the input spline

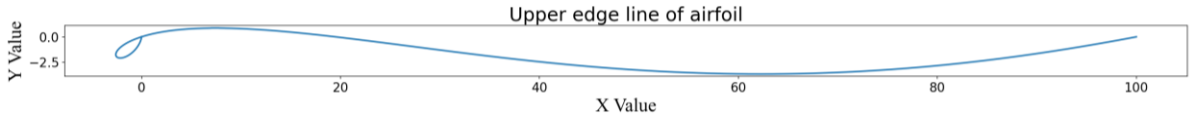

Fig. 16 Generated upper arc

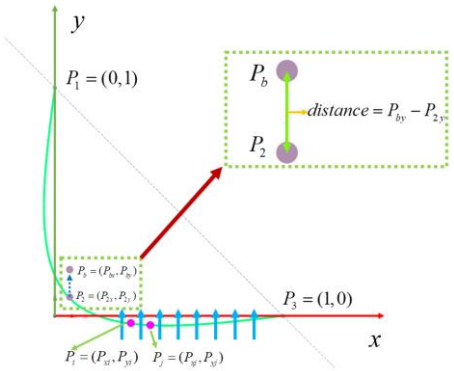

Fig. 17 Spline curve optimization algorithm

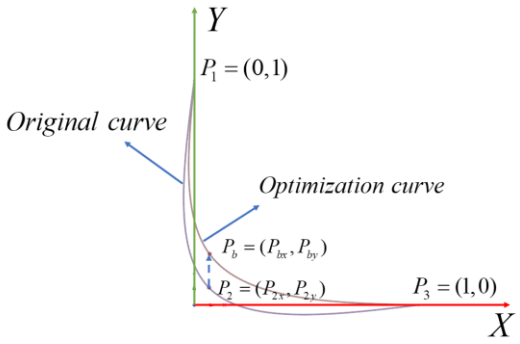

Fig. 18 Original and the optimized spline curves

curve for the upper curve of the airfoil. In this study, the approach of moving point P_2 in the positive direction of the vertical axis is adopted to manipulate the spline curve. The figure on the right demonstrates the result after the manipulation. The optimization algorithm is illustrated in Fig. 17.

Firstly, the interval point information is processed based on the analysis results, and P_2 is moved in the direction of the Y-axis. As P_2 moves, the spline curve between P_1 and P_3 will also move accordingly. In this case, the movement of P_2 to the position P_b must satisfy the following computational conditions:

$$distance = P_{by} - P_{2y} \tag{10}$$

$$distance = min(P_y) + n\Delta t, \Delta t = 0.1\left|min(P_y)\right| \tag{11}$$

$$K_{P_iP_j} = \frac{P_{yj} - P_{yi}}{P_{xj} - P_{xi}}, K_{P_iP_j} < 0 \tag{12}$$

where, n represents the number of times to control the range of movement of point P_2. P_i and P_j represent any two adjacent points between P_2 and P_3, and their coordinate values must satisfy a decreasing condition determined by formula 12. If this condition is not met, the value of n needs to be modified, and the input curve optimization process should be repeated. The original spline curve and the optimized spline curve are shown in Fig. 18.

The optimized spline curve is taken as the input curve to generate the upper arc curve. The generated upper arc curve with the optimization is illustrated in Fig. 19.

From Fig. 19, it can be observed that the optimized upper curve significantly complies with the requirements of airfoil design. By extending the research on this design method, as shown in Fig. 20, 90 airfoil upper curves are generated. The generated airfoil upper curves are smooth, and most of them are reasonably satisfactory.

To investigate the relationship between the position of points on the wing profile with a curvature of zero and the coordinates of the middle control points in the input curve, according to the middle control point generation rules (Equations 7, 8, 9), it is sufficient to investigate the vertical coordinate of the middle control point P_2 and its positional relationship with the angle α and the points on the wing profile with a curvature of zero. Firstly, 10,000 wing profile samples are generated, and the coordinates of the middle control point and the points on the wing profile with a curvature of zero are preprocessed. Within a certain range of y-values, the effects of α and the vertical coordinate of the middle control point on the horizontal and vertical coordinates of the points on the wing profile with a curvature of zero are discussed separately.

As illustrated in Fig. 21, the rationality and generation speed of the composite spline curve are considered. When the value range of y is set to $0.25 \le y \le 0.76$, as the value of α increases, the abscissa of the point where the rate of change of the arc on the wing shape is zero increases gradually, demonstrating a predominantly monotonic increasing characteristic. When $y \ge 0.67$, there is a sudden change in the curve's trailing edge.

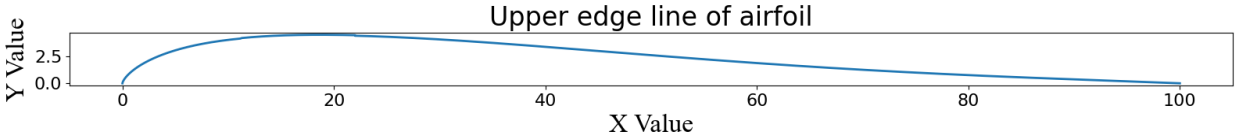

Fig. 19 Optimized upper arc

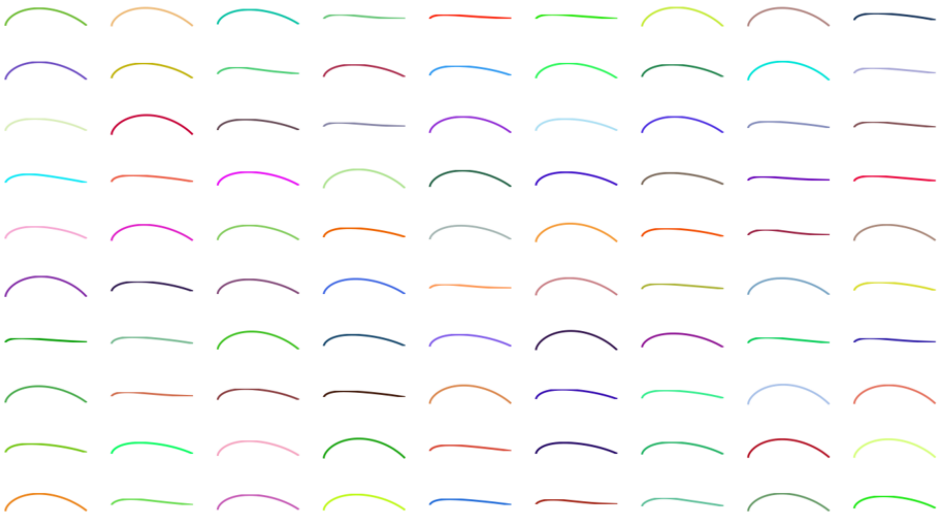

Fig. 20 90 airfoil upper arcs

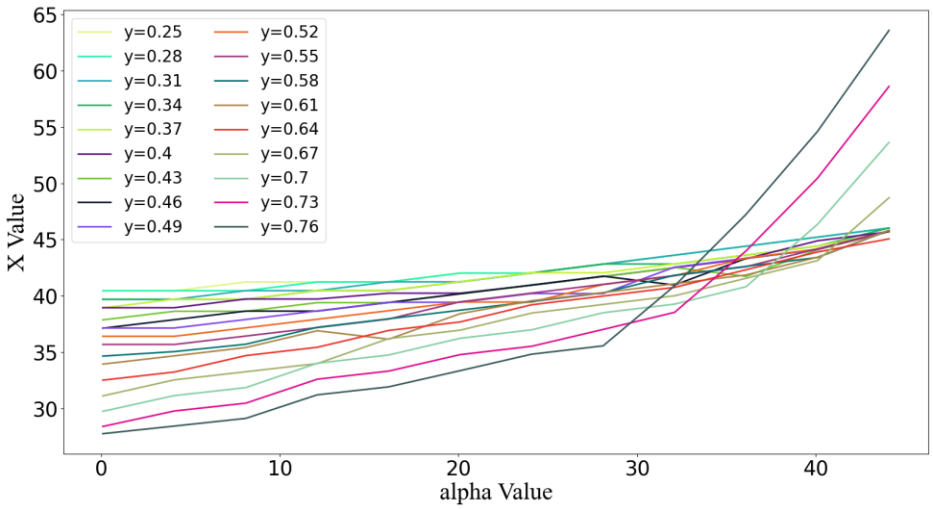

Fig. 21 Relation between α value and the point with zero rate of arc change on airfoil

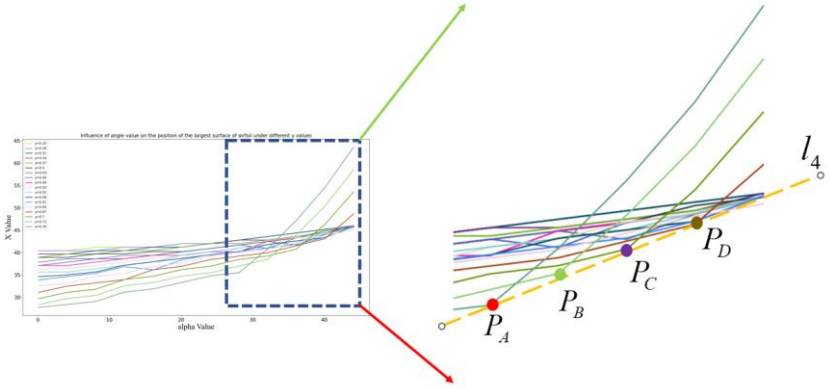

Fig. 22 Analysis of mutation points

Among these, the four points P_A, P_B, P_C, and P_D denote the starting positions of the discontinuity, and both the value of α and the abscissa of the discontinuity decrease gradually with the increasing y-value, demonstrating a linear relationship between the four discontinuity stages, as illustrated in Fig. 22.

Through statistical analysis of the generated airfoil, it is found that the horizontal coordinate range of the point with the maximum curvature on the upper arc of the airfoil

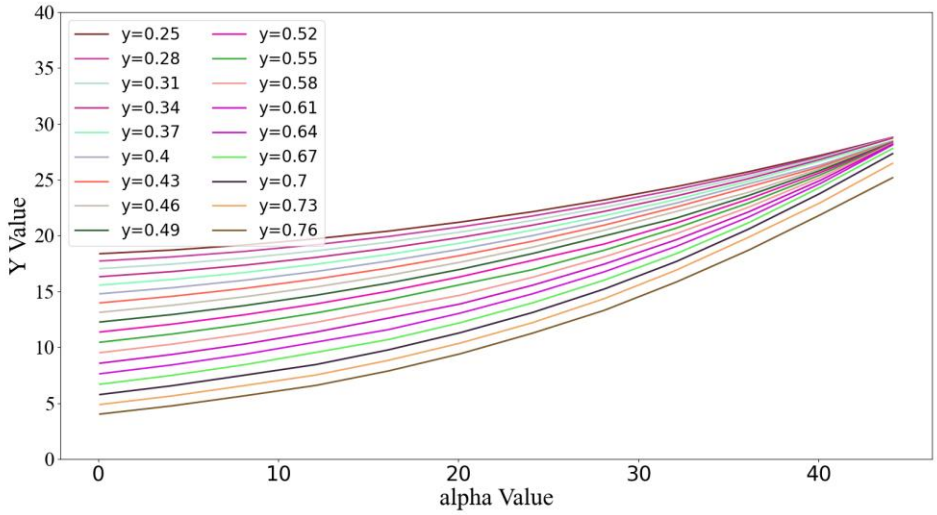

Fig. 23 Relationship between the value of α and the ordinate of the curve where the change rate of the airfoil is zero

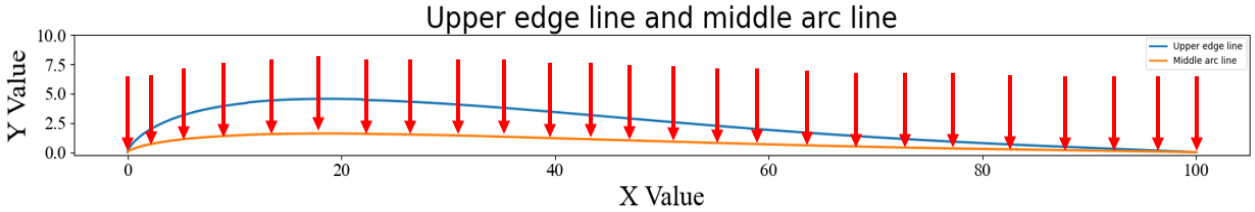

Fig. 24 Determination of the middle arc

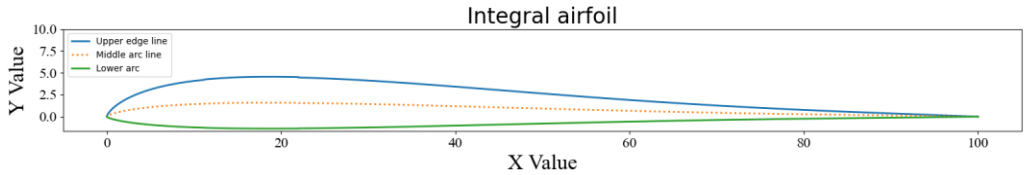

Fig. 25 Overall airfoil curve

satisfies the required criteria. The relationship between the vertical coordinate of the point where the curvature of the upper arc of the airfoil is zero and α is presented in Fig. 23. Under different y values, as the value of α increases, the vertical coordinate values of the point where the curvature of the upper arc of the airfoil is zero grow exponentially.

Through a comprehensive analysis of the three methods for generating the upper contour of the airfoil based on the aforementioned input curves, it is found that the third method using the control point spline curve exhibits the fastest speed, highest sample quantity, and perfect preservation of the input curve features. Meanwhile, when the positions of the randomly generated control points are not reasonable, curve optimization and reconstruction can be achieved through rapid control point translation.

4. THE GENERATION OF AIRFOIL LIBRARIES

Based on the generation of upper curved arcs, a design methodology for the mid-arc has been proposed. The overall wing profile is obtained by controlling the wing profile thickness. Meanwhile, a method for generating composite wing profiles is proposed to enhance the wing profile characteristics.

4.1 Middle arc Design Method

Taking the optimized upper arc curve in Section 2.2 as an example, the control concept is to scale the ordinate of the upper arc curve. Figure 24 illustrates the resulting middle arc curve, which is generated by scaling the ordinate of the original upper arc curve by 35 percent.

4.2 Integral Airfoil Generation

Following the definition of the wing airfoil's middle curve, the coordinates of the upper curve and middle curve are interpolated and averaged to obtain the position coordinates of the lower curve. The lower curve is generated by combining the upper curve and the lower curve. The overall wing airfoil curve is presented in Fig. 25.

4.2.1 Airfoil Thickness Control

The maximum height of the upper arc determines the maximum potential thickness that the overall airfoil can achieve, and the maximum gap between the upper arc and middle arc determines the thickness of the entire airfoil.

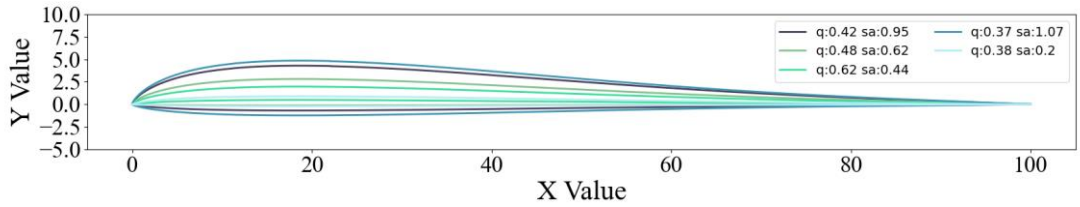

Fig. 26 Five airfoil curves

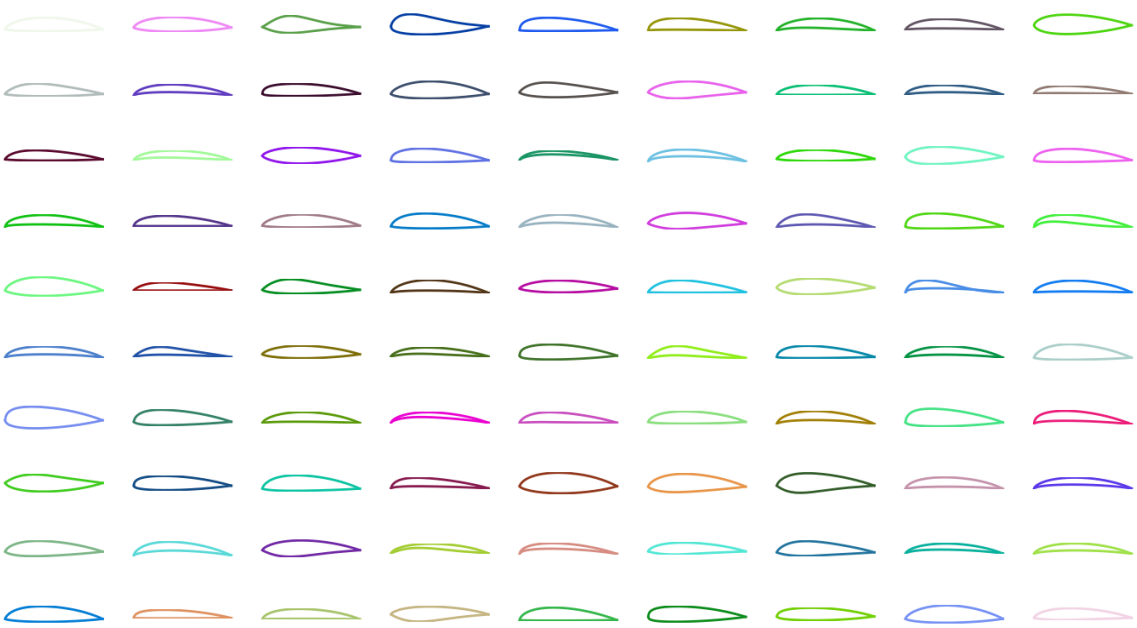

Fig. 27 90 airfoils based on the random recombination of the edges of 10,000 types of upper and lower arcs

Therefore, before determining the overall shape of the airfoil, it is necessary to determine the position of the maximum thickness coordinate point on the upper arc, specify the target thickness, and determine the position of the middle camber in reverse order, thereby forming the mean camber line. To better optimize the thickness of the airfoil, this paper defines a thickness control formula in the following form:

$$T = 2S_a Y_i (1-q) \tag{13}$$

where, S_a denotes the scaling factor for the maximum thickness of the upper curve, $S_a > 0$, Y_i denotes the ordinate of the control point of the upper curve, and q is a scaling factor. Figure 26 shows five wing profile curves generated with different settings of control thickness factors S_a and q. It can be clearly seen that not only the wing thickness can be accurately controlled, but also the shape of the wing profile can be transformed. By comparing and selecting a large amount of generated wing profile simulation data, it is found that the variation in the irregular curve is more pronounced when q falls within the range [0.37,0.71]. Therefore, the interval of [0.37,0.71] is selected for display in Fig. 26.

4.2.2 Airfoil Library Generation

The section presents a method for generating a large range of airfoil contours so that an airfoil library can be established. Based on the aforementioned wing generation approach, research on wing generation can be conducted by using existing wing algorithms to control the generation of upper and lower wing profiles for all wing shapes. The upper and lower profiles are stored separately in sets *A* and *B*, respectively. Then, profiles are randomly selected from sets *A* and *B* for recombination. In principle, assuming set *A* has *m* upper arcs and set *B* has *n* lower arcs, this leads to a total of *m***n* wing shape libraries. Figure 27 demonstrates 90 wing shapes obtained by randomly recombining the upper and lower profiles of 10,000 wing shapes. These wing shapes exhibit more diverse characteristics.

5. VALIDATION AND ANALYSIS

To verify the compliance of the proposed wing design method with aerodynamic performance requirements, a standardized wing profile is randomly selected for analysis, with reference to the wind tunnel data of a certain wing type.

5.1 Generation of Airfoils with Different Thickness Ranges

The specific parameter settings of the selected airfoil are as follows: the maximum thickness position and maximum camber position are at 28.53% of the chord length. The airfoil thickness is taken as the optimization variable, the thickness varies with an initial value of 2.52% of the chord length. The variation in airfoil thickness is indicated by the blue arrow in Fig. 28, with the final thickness at 17.64% of the chord length.

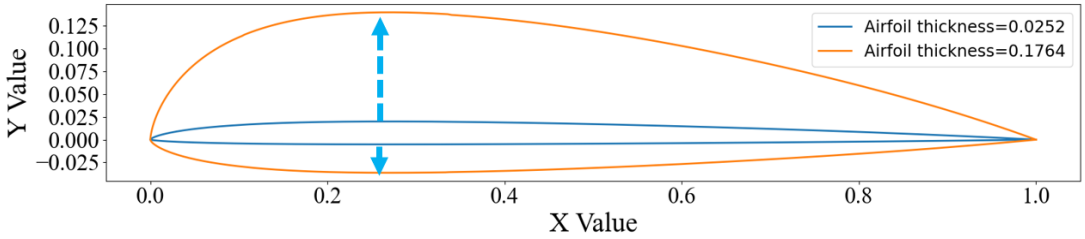

Fig. 28 Airfoils with different thickness ranges

To guarantee the smoothness of the wing surface, a reverse processing operation is adopted. Firstly, the smoothing operation is performed in the XFOIL program, followed by re-outputting the wing coordinates. This section focuses only on reliable validation of the self-designed airfoil and presents an optimization method that utilizes Python + XFOIL for preliminary rapid optimization to select reasonable airfoil shapes. Then, an accurate analysis model is constructed using Ansys Fluent to calculate the precise aerodynamic parameters of the initially optimized airfoil.

A total of 1000 airfoil shapes with equidistantly selected initial and final thicknesses are generated. The airfoil thickness is taken as the optimization parameter, and the maximum lift-to-drag ratio is taken as the objective parameter. Owing to the fast calculation speed of the XFOIL program, it satisfies the requirement for batch processing optimization. Therefore, the optimal thickness airfoil is first computed using Python to invoke the XFOIL program and determine the airfoil with the highest lift-to-drag ratio. Next, Fluent is employed to construct a wind tunnel space for the two-dimensional airfoil, enabling a more detailed analysis of the airfoil optimized by XFOIL. The lift-to-drag characteristics of the optimized airfoil are provided, which lays the technical foundation for subsequent three-dimensional wing design.

5.2 Rapid Airfoil Selection Based on XFOIL Software

An optimal aerodynamic performance curve needs to be selected from the airfoil generated in Section 5.1, to achieve rapid selection through the XFOIL software.

When adding a Reynolds number of 6e+6, an angle of attack of 2°, and a Mach number of 0.15, the variation of lift-to-drag ratio for the airfoil within the thickness between 2.52% and 17.62% of the chord length is shown in Fig. 29. It can be observed that as airfoil thickness increases, the lift-to-drag ratio initially increases and then gradually stabilizes, and finally, it decreases with a further increase in airfoil thickness. The green triangle and red triangle points in Fig. 29 correspond to the airfoil thicknesses of 10.18% and 13.09% of the chord length, respectively, with both exhibiting a maximum lift-to-drag ratio of 97.59. Therefore, further investigation is performed on the two airfoil thicknesses corresponding to the two largest lift-to-drag ratios in the figure. Relatively thicker airfoils exhibit greater structural strength but lead to increased weight and cost. Therefore, it is necessary to further optimize the structural strength of three-dimensional wings in future research.

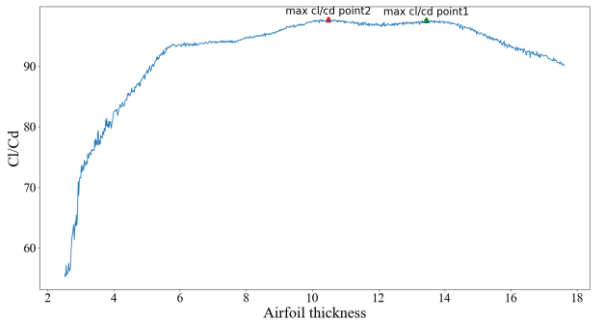

Fig. 29 Relationship between Cl/Cd and thickness parameters

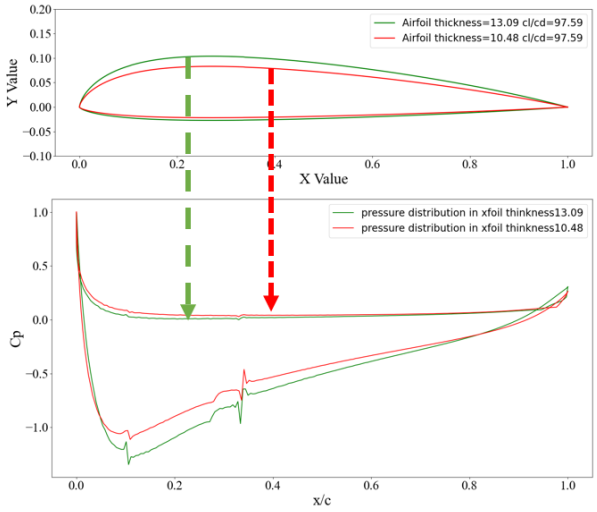

Fig. 30 Airfoil and gauge pressure curves

Figure 30 presents the airfoil shapes and corresponding pressure distribution curves of green and red points. Though the lift-to-drag ratios for both airfoil shapes are almost identical, the pressure distribution plot illustrates that the airfoil with a thickness of 10.48% exhibits a smoother pressure distribution and more gradual fluctuation, demonstrating superior aerodynamic characteristics compared to the airfoil with a thickness of 13.09%.

Therefore, the wing profile with a thickness of 10.18% is selected for further analysis, as shown in Fig. 31.

5.3 Comparison of Verification Results

This section compares the lift-to-drag ratio of the airfoil obtained in Section 5.2 with the results in the literature

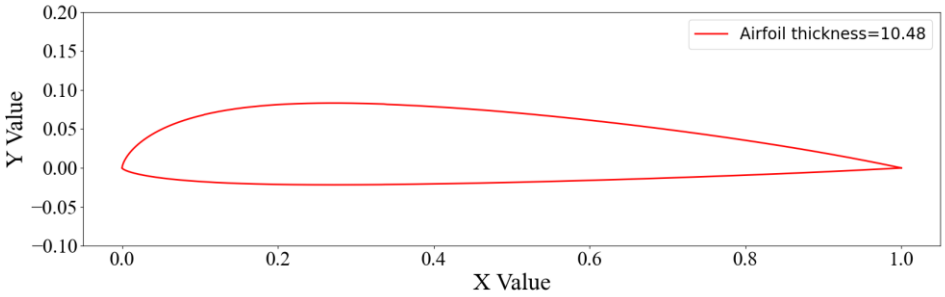

Fig. 31 The optimized airfoil

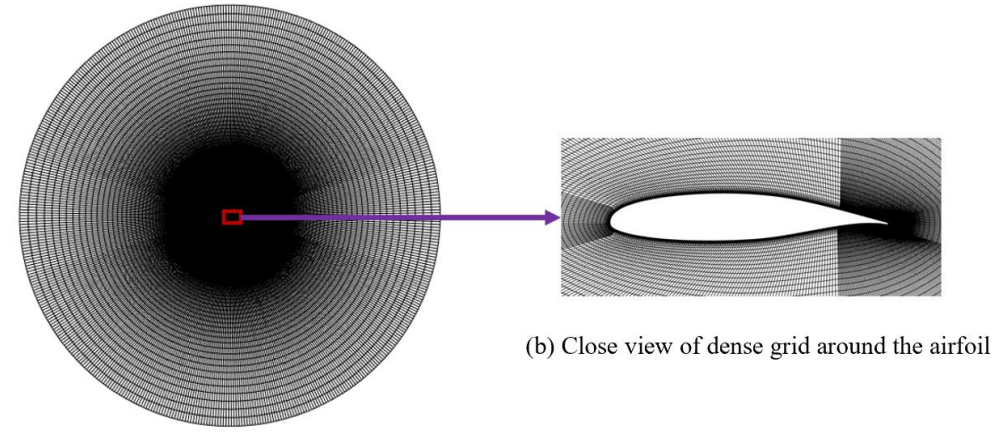

(a) Far view of structured grid in the domain with boundary conditions

(b) Close view of dense grid around the airfoil

Fig. 32 Comparison between the flow field grid model and its own model

(Ribeiro et al., 2012). Meanwhile, the airfoil experimental data and airfoil studied in the literature (McGhee, 1980; Ribeiro et al., 2012) are taken as the research model to verify the effectiveness of the Fluent calculation model and ensure the accuracy of the subsequent optimization of the independent design model.

Fluent 2023 R1 is employed as a simulation tool in this section, and the experiments in the literature are verified. In the test, far-field boundary conditions were employed, and a Shear-Stress Transport (SST) k-ω model was adopted, the attack angle is 8.02°, the Mach number is 0.15, the Reynolds number is 6e+6 for the setting condition, and the far-field distance is equal to 340 times the string length.

The verification process begins with the establishment of the flow field grid model, and Python is used to create the grid in the study.

The computational domain for simulation is illustrated in Fig. 32 (a). These grids are created following the first-tier grid height computing theory and have the following characteristics:

(1) the grid height of the first layer of the airfoil surface is *y*.

(2) the ratio of height variation from the airfoil surface to the far-field boundary grid is 1.1.

(3) the diameter of the calculation domain is set to 340 times the chord length to achieve a fully developed flow.

(4) the surface mesh size of the airfoil is 3, and there are 110 nodes in the far field radius.

Based on the pressure data and lift-to-drag ratio data obtained from simulations and experiments in the references, pressure coefficient graphs were generated by comparing the XFOIL and Fluent models in this study with the experimental model, as shown in Fig. 33. The simulated results closely match the experimental results in terms of pressure coefficient, particularly for the Fluent model, which demonstrates a high level of agreement with the experimental data. Though the pressure coefficient graph obtained from the XFOIL program is slightly different from both the Fluent model and the experimental results in the vicinity of the maximum pressure location on the upper curve of the airfoil, the overall trends are consistent. Therefore, it can be inferred that utilizing the XFOIL program for preliminary optimization is compliant with computational standards.

Then, by using the aforementioned model, the lift-to-drag ratio curves were calculated, as shown in Fig. 34. The reference data for comparison were obtained from the reference (Ribeiro et al., 2012). The value ranges for attack angle and lift-to-drag ratio are [-8.02, 12.04] and [-50, 100], respectively. After precise fluent modeling of the designed airfoil, the Euclidean distance between the wind tunnel data and our modeled data is 0.0331. In contrast, the Euclidean distance between the simulation data in the reference literature and the wind tunnel data is 0.0408.

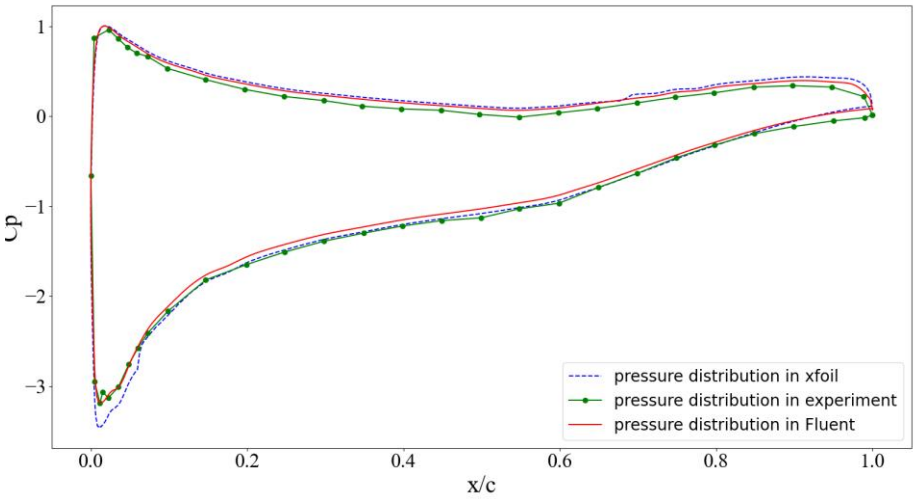

Fig. 33 Pressure coefficient

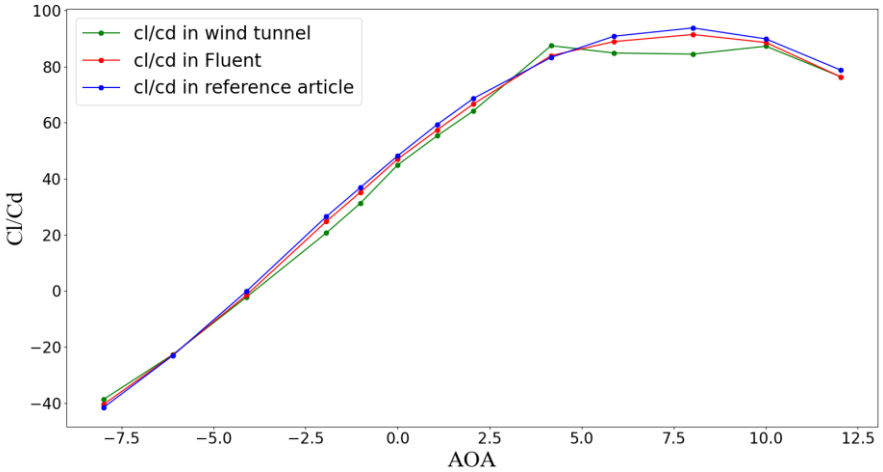

Fig. 34 Curve of the lift-drag ratio

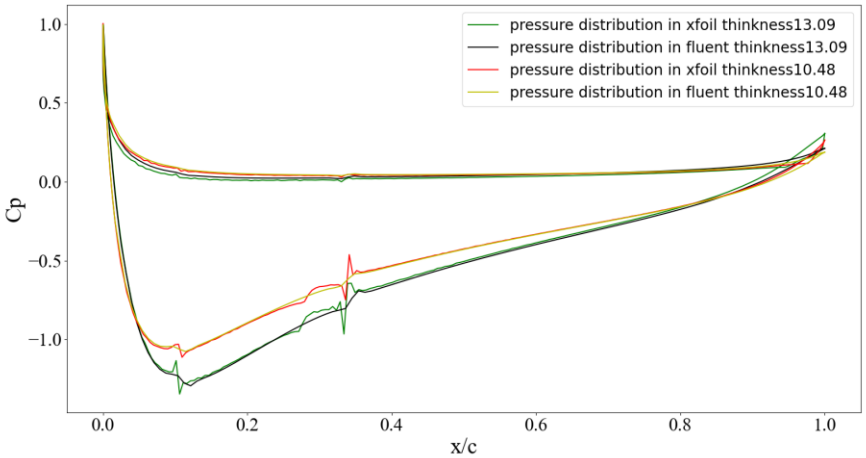

Fig. 35 Pressure coefficient distribution results

Therefore, our precision model achieves 18.9% higher accuracy than the literature model, with a higher curve similarity. Thus, this validation model exhibits good precision and provides support for accurate computational models in future research.

The pressure coefficient calculations were performed on airfoils with thicknesses of 10.18% and 13.09% respectively, and the results are illustrated in Fig. 35. From this figure, it can be observed that the pressure coefficient distributions obtained from the Fluent computational model exhibit a high degree of consistency with those obtained from the XFOIL program. However, the pressure coefficient distribution curves obtained from the XFOIL program are not as smooth as those obtained from the Fluent model. This further confirms the validity of using

the XFOIL program for rapid selection and then the Fluent computational model for detailed optimization, thus laying a sound technical foundation for airfoil selection in subsequent three-dimensional wing design.

6. Conclusion

Based on mathematical computation and geometric thinking, this paper proposes an original wing design method and develops an optimization algorithm that combines Python programming. The XFOIL program is utilized to generate wing profiles in batch processing, and the optimal wing profile is output based on the lift-to-drag ratio as the optimization objective. Besides, a precise Fluent analysis model is established. The main conclusions of this paper are as follows:

(1) The upper arc line is optimized by combining mathematical computation and geometric thinking. This method has strong scalability. By designing different concave functions with a 0-1 distribution, various upper arc lines can be obtained.

(2) An airfoil library generation method is proposed. The lower profile line is determined by the contour line of the upper wing profile and the middle curve, allowing precise control of the wing thickness. Meanwhile, by adding a random control factor to the wing thickness, many different wing profiles can be generated. Then, the contour lines of the upper and lower wing profiles are randomly combined to enrich the generated airfoil profile library.

(3) The aerodynamic performance of the devised airfoil is validated by XFOIL and Fluent tools. An optimization algorithm is designed to select the optimal wing profile from multiple wings with equal thickness. Also, a Fluent model is established for accuracy analysis. Besides, comparative verification is carried out using the research wing profile from literature data, with the attack angle ranging from [-8.02, 12.04] and the lift-to-drag ratio ranging from [-50, 100]. After accurate Fluent modeling, it is found that the Euclidean distance between the designed wing profile and wind tunnel data is 0.0331, while the Euclidean distance between the simulated data in literature and wind tunnel data is 0.0408. The proposed model achieves 18.9% higher accuracy than the model in the literature, and the curve similarity is higher. The results indicate that the proposed integral airfoil profile generation algorithm based on upper airfoil contour optimization has significant advantages in terms of accuracy and overall analysis speed while exhibiting high scalability.

Acknowledgements

This research was funded by the Scientific and technological innovation project, KYGYZXJK150025; Youth Fund of the National Natural Science Foundation of China (62103441)

Conflict of Interest

The authors declare no conflict of interest.

Authors Contribution

Conceptualization. **Z. Wang**, **W. B. Gu** and **Q. Yuan**; methodology, **Q. Yuan** and **X. B. Xie**; software, **Z. Wang** and **X. B. Xie**; validation, **Q. Yuan**; formal analysis, **Z. Wang**; investigation, **Q. Yuan**; resources, **Z. Wang**; data curation, **Z. Wang** and **Y. Zhu**; writing—original draft preparation, **Z. Wang** and **Y. Zhu**; writing—review and editing, **Q. Yuan** and **X. B. Xie**; visualization, **Z. Wang** and **W. B. Gu**; supervision, **Q. Yuan**, **Y. Zhu** and **W. B. Gu**; project administration, **Q. Yuan** and **Y. Zhu**; funding acquisition, **Q. Yuan** and **W. B. Gu**. All authors have read and agreed to the published version of the manuscript.

References

Aghabeigi, M., Khodaygan, S., & Movahhedy, M. R. (2022). Tolerance analysis of a compliant assembly using random Non-Uniform Rational B-Spline curves and isogeometric method. *Journal of Computational Design and Engineering*, *9*(6), 2170-2195. https://doi.org/10.1093/jcde/qwac093.

Akram, M. T., & Kim, M. H. (2021). Aerodynamic shape optimization of NREL S809 airfoil for wind turbine blades using Reynolds-averaged Navier stokes model—Part II. *Applied Sciences*, *11*(5), 2211. https://doi.org/10.3390/app11052211.

Bharadwaj, P., Mulder, W., & Drijkoningen, G. (2016). Full waveform inversion with an auxiliary bump functional. *Geophysical Journal International*, *206*(2), 1076-1092. https://doi.org/10.1093/gji/ggw129.

Buckley, H. P., & Zingg, D. W. (2013). Approach to aerodynamic design through numerical optimization. *AIAA Journal*, *51*(8), 1972-1981. https://doi.org/10.2514/1.J052268.

Chen, X., & Agarwal, R. K. (2014). Shape optimization of airfoils in transonic flow using a multi-objective genetic algorithm. *Proceedings of the Institution of Mechanical Engineers, Part G: Journal of Aerospace Engineering*, *228*(9), 1654-1667. https://doi.org/10.1177/0954410013500613.

Fujii, K., & Dulikravich, G. (Eds.). (2013). *Recent Development of Aerodynamic Design Methodologies: Inverse Design and Optimization* (Vol. 65). Springer Science & Business Media.

Gardner, B., & Selig, M. (2003, January). Airfoil design using a genetic algorithm and an inverse method. 41st Aerospace Sciences Meeting and Exhibit (p. 43). https://doi.org/10.2514/6.2003-43.

Guibault, F., Bentamy, A., & Trépanier, J. Y. (2002). Constraints specifications on NURBS Surfaces for Wing Geometric Representation. *9th AIAA/ISSMO Symposium on Multidisciplinary Analysis and Optimization* (p. 5400). https://doi.org/10.2514/6.2003-43.

Hicks, R. M., & Henne, P. A. (1978). Wing design by numerical optimization. *Journal of Aircraft, 15*(7), 407-412. https://doi.org/10.2514/3.58379.

Huang, D., Allen, T. T., Notz, W. I., & Zeng, N. (2006). Global optimization of stochastic black-box systems via sequential kriging meta-models. *Journal of Global Optimization, 34*, 441-466. https://doi.org/10.1007/s10898-005-2454-3.

Khurana, M., Winarto, H., & Sinha, A. (2008, October). *Application of swarm approach and artificial neural networks for airfoil shape optimization*. *12th AIAA/ISSMO Multidisciplinary Analysis And Optimization Conference* (p. 5954). https://doi.org/10.2514/6.2008-5954.

Kou, J., Botero-Bolívar, L., Ballano, R., Marino, O., de Santana, L., Valero, E., & Ferrer, E. (2023). Aeroacoustic airfoil shape optimization enhanced by autoencoders. *Expert Systems with Applications*, *217*, 119513. https://doi.org/10.48550/arXiv.2210.00101.

Kulfan, B. M. (2008). Universal parametric geometry representation method. *Journal of Aircraft, 45*(1), 142-158. https://doi.org/10.2514/1.29958.

Lee, K. D., & Eyi, S. (1992). Aerodynamic design via optimization. *Journal of Aircraft, 29*(6), 1012-1019. https://doi.org/10.2514/3.46278.

Lepine, J., Guibault, F., Trepanier, J. Y., & Pepin, F. (2001). Optimized nonuniform rational B-spline geometrical representation for aerodynamic design of wings. *AIAA Journal, 39*(11), 2033-2041. https://doi.org/10.2514/2.1206.

Leung, T., & Zingg, D. (2009). *Single-and multi-point aerodynamic shape optimization using a parallel Newton-Krylov approach. 19th AIAA Computational Fluid Dynamics* (p. 3803). https://doi.org/10.2514/6.2009-3803.

Li, J., Zhang, M., Tay, C. M. J., Liu, N., Cui, Y., Chew, S. C., & Khoo, B. C. (2022). Low-Reynolds-number airfoil design optimization using deep-learning-based tailored airfoil modes. *Aerospace Science and Technology, 121*, 107309. https://doi.org/10.1016/j.ast.2021.107309.

Li, M., Liu, X., Jia, D., & Liang, Q. (2015). Interpolation using non-uniform rational B-spline for the smooth milling of ruled-surface impeller blades. *Proceedings of the Institution of Mechanical Engineers, Part B: Journal of Engineering Manufacture*, *229*(7), 1118-1130. https://doi.org/10.1177/0954405415586966.

McGhee, R. J. (1980). *Low-speed aerodynamic characteristics of a 17-percent-thick medium speed airfoil designed for general aviation applications*. National Aeronautics and Space Administration, Scientific and Technical Information Branch.

Mengistu, T., & Ghaly, W. (2002). *A geometrical representation of turbomachinery cascades using NURBS. 40th AIAA Aerospace Sciences Meeting & Exhibit* (p. 318). https://doi.org/10.2514/6.2002-318.

Nemec, M., Zingg, D. W., & Pulliam, T. H. (2004). Multipoint and multi-objective aerodynamic shape optimization. *AIAA Journal, 42*(6), 1057-1065. https://doi.org/10.2514/1.10415.

Painchaud-Ouellet, S., Tribes, C., Trépanier, J. Y., & Pelletier, D. (2006). Airfoil shape optimization using a nonuniform rational b-splines parametrization under thickness constraint. *AIAA Journal, 44*(10), 2170-2178. https://doi.org/10.2514/1.15117.

Prautzsch, H., Boehm, W., & Paluszny, M. (2002). *Bézier and B-spline techniques* (Vol. 6). Berlin: Springer.

Ramamoorthy, P., & Padmavathi, K. (1977). Airfoil design by optimization. *Journal of Aircraft, 14*(2), 219-221. https://doi.org/10.2514/3.44587.

Ribeiro, A. F. P., Awruch, A. M., & Gomes, H. M. (2012). An airfoil optimization technique for wind turbines. *Applied Mathematical Modelling, 36*(10), 4898-4907. https://doi.org/10.1016/j.apm.2011.12.026.

Sekar, V., Zhang, M., Shu, C., & Khoo, B. C. (2019). Inverse design of airfoil using a deep convolutional neural network. *AIAA Journal, 57*(3), 993-1003. https://doi.org/10.2514/1.J057894.

Sevilla, R., Fernández-Méndez, S., & Huerta, A. (2011). NURBS-enhanced finite element method (NEFEM) a seamless bridge between CAD and FEM. *Archives of Computational Methods in Engineering, 18*, 441-484. https://doi.org/10.1007/s11831-011-9066-5.

Sun, G., Sun, Y., & Wang, S. (2015). Artificial neural network based inverse design: Airfoils and wings. *Aerospace Science and Technology, 42*, 415-428. https://doi.org/10.1016/j.ast.2015.01.030.

Vicini, A., & Quagliarella, D. (1997). Inverse and direct airfoil design using a multiobjective genetic algorithm. *AIAA Journal, 35*(9), 1499-1505. https://doi.org/10.2514/2.274.

Wang, G., Chen, Q., & Zhou, M. (2004). NUAT B-spline curves. *Computer Aided Geometric Design, 21*(2), 193-205. https://doi.org/10.1016/j.cagd.2003.10.002.

Zakaria, R., Wahab, A. F., Ismail, I., & Zulkifly, M. I. E. (2021). Complex uncertainty of surface data modeling via the type-2 fuzzy B-spline model. *Mathematics*, 9(9), 1054. https://doi.org/10.3390/math9091054.

Zhang, T. T., Wang, Z. G., Huang, W., & Yan, L. (2018). A review of parametric approaches specific to aerodynamic design process. *Acta Astronautica, 145*, 319-331. https://doi.org/10.1016/j.actaastro.2018.02.011.

Zhou, H., Zhou, S., Gao, Z., Dong, H., & Yang, K. (2021). Blades optimal design of squirrel cage fan based on Hicks-Henne function. *Proceedings of the Institution of Mechanical Engineers, Part C: Journal of Mechanical Engineering Science*, 235(19), 3844-3858. https://doi.org/10.1177/0954406220969728.